



Thermal and entropy generation of non-Newtonian magneto-Carreau fluid flow in microchannel

S. A. Shehzad¹ · Macha Madhu² · N. S. Shashikumar³ · B. J. Gireesha² · B. Mahanthesh⁴

Received: 24 January 2020 / Accepted: 13 April 2020 / Published online: 30 April 2020
© Akadémiai Kiadó, Budapest, Hungary 2020

Abstract

The heat flow in microchannels can be established in numerous applications such as micro air vehicles, mechanical–electromechanical systems, cooling of electronic devices and micro heat exchanger systems. Heat flow optimization deliberates the function of entropy generation minimization (EGM) in engineering applications. Hence, this paper investigates the heat transport of non-Newtonian magneto-Carreau fluid in a microchannel with EGM. Mathematical modeling incorporates the Carreau fluid model. Further, viscous heating, Joule heating and convective heating aspects are also analyzed. The physical features of entropy production in the flow of non-Newtonian Carreau fluid in a microchannel are the major focus of this model. Dimensionless variables are executed for the simplicity of basic equations. The subsequent system is treated by using finite element method. Behaviors of effective parameters on velocity, Bejan number, entropy generation rate and temperature are interpreted. It is established that EGM is occurred for larger values of Weissenberg number. The Carreau fluid exponent is positively related to Bejan number, whereas it is negatively related to EG, temperature and velocity fields.

Keywords Entropy generation · Carreau fluid · Magnetic field · Bejan number · Magnetic field · Microchannel

Introduction

It is well-known fact that the distinct liquids used in our daily routine and industry differ from the rheology of Newtonian materials. Such distinct liquids are termed as “Newtonian fluids.” Examples of such materials are juices, shampoos, blood, toothpaste, ketchup, sugar solutions, polymer solutions, drilling muds, lubricants oils, slurries, soaps and many others. There is not a single mathematical formula which addresses the complete nature of these materials. The non-Newtonian fluids have abundant implications in science and engineering fields such as blade and wire coating, dyeing of textiles and papers, plastic manufacturing, motion

of biological liquids and food processing. The nature of such fluids has attained the focal involvement of the researchers to discuss the dynamics and rheology. The researchers had established distinct mathematical relationships for different rheological behavior fluids. Among multiple non-Newtonian models, we involved the Carreau fluid for recent research demonstration. This model is very complex and nonlinear and very popular among the present researchers [1–10].

The main objective in the designing of thermal devices is the efficient energy implication. This can be made through the entropy generation minimization (EGM) in the processes of thermal devices. The development of heat removal machines and energy optimization require the minimization of entropy destruction and production because of work by viscous friction, heat transport and conduction of electric field. The available energy efficacy can be more desirable via the optimization of entropy production. Chamkha et al. [11] studied the thermal analysis and MHD copper (Cu)–water (H₂O) nanofluid flow in a porous enclosure. Mehryan et al. [12] executed the analysis of EG in ferromagnetic fluid through square enclosure under horizontal Lorentz force. Shamsabadi et al. [13] inspect the thermal and viscous irreversibilities of nanofluid inside a duct geared up with porous baffles. Seyyedi et al. [14] reported the radiative EG of Cu–water nanoparticles flow in semi-annulus

✉ B. Mahanthesh
mahanthesh.b@christuniversity.in

¹ Department of Mathematics, COMSATS University Islamabad, Sahiwal 57000, Pakistan

² Department of Mathematics, Kuvempu University, Shimoga, India

³ Department of Mathematics, Malnad College of Engineering, Hassan 573202, India

⁴ Department of Mathematics, CHRIST (Deemed to be University), Bangalore 560029, India

cavity. Abbasi et al. [15] developed the EG model of peristaltic flows through long-wavelength theory. They also reported the temperature-dependent characteristics of viscosity and Hall phenomenon. Shafee et al. [16] addressed the EG analysis for magnetized ferrofluid induced by semi-porous annulus. They reported that the system disorder is enhanced due to Darcy constraint. The EG under viscous heating flow of peristaltic fluid in channel has been numerically described by Abbasi et al. [17]. Sheikholeslami [18] described the EG and exergy analysis in nanofluid through Lorentz force in porous space. Bahrami et al. [19] discussed the spectral analysis of EG in non-gray planer medium. Hayat et al. [20] demonstrated the statistical analysis of EG in nanomaterial flow induced by the rotation of two disks. They also computed the statistical and probable error in this study. Recently, the same theory has been interestingly used by many researchers with different perspectives [21–26].

In present, many practical and theoretical studies are conducted on the microfluidic systems. The applications microfluidic is in micro pumps, micro device, micro mixer, polymers, biomedical micro cell and MCHS. Venkateswarlu et al. [27] studied the effect of slip velocity boundary condition with the temperature jump under influence of magnetic field. The impact of heat generation and thermal radiation by considering slip velocity boundary condition and temperature jump on the channel walls was investigated by Venkateswarlu [28]. Monal-edi and Makinde [29] numerically studied Cu–water nanofluid flow inside a microchannel in the presence of nanoparticles shape effect. Madhu et al. [30] numerically studied steady, laminar and nanofluid flow inside a horizontal microchannel by implementing finite element method. The fluid flow in microchannel has been investigated in recent studies [31, 32].

This research focusses on the thermal and entropy minimization features in laminar non-Newtonian magneto-Carreau fluid. The fluid flows through convectively heated microchannel. The combined consideration of entropy and magnetic field on Carreau fluid in microchannel has not been addressed in the

literature. Further, the involvement of convective heating process strengthened this research. The simplified expressions are converted to dimensionless model with the help of appropriate variables. These expressions are executed with the implication of finite element scheme. The outcomes of these expressions are labeled for distinct values of arising constraints to address the behavior of Bejan number, temperature and velocity local rate of entropy generation.

Mathematical development and solution

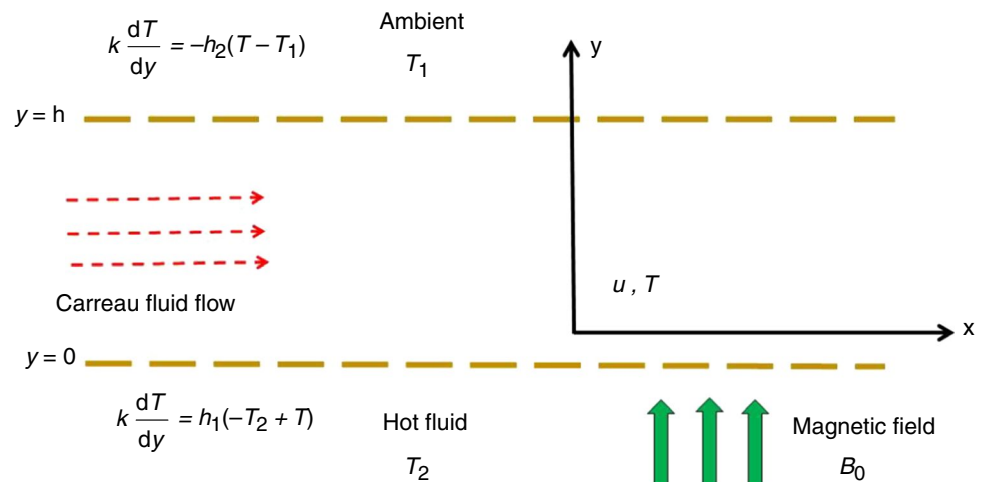
Flow and heat transport

A fully developed dissipative, incompressible, electrically conducting non-Newtonian Carreau fluid flow between two fixed permeable infinite plates of microchannel of width h is considered. The below plate is at transversal coordinate $y = 0$ and upper plate is at $y = h$ (see Fig. 1). An unvarying magnetic potency with strength B_0 is imposed transversely to the plates. Suction takes place at upper plate, while the liquid is injected at lower plate. The right plate of microchannel has connection with ambient temperature T_1 , while the below plate interchanges heat through convection with hotter fluid of temperature T_2 . Based on the above suppositions, the governing balances for non-Newtonian Carreau fluid are given as follows:

$$\frac{dv}{dy} = 0, \quad (1)$$

$$\begin{aligned} \rho v_0 \frac{du}{dy} = & -\frac{dp}{dx} + \mu \frac{d^2u}{dy^2} \left(1 + \Gamma^2 \left(\frac{du}{dy} \right)^2 \right)^{\left(\frac{n-1}{2}\right)} \\ & + \mu(n-1) \Gamma^2 \frac{d^2u}{dy^2} \left(1 + \Gamma^2 \left(\frac{du}{dy} \right)^2 \right)^{\left(\frac{n-3}{2}\right)} \left(\frac{du}{dy} \right)^2 - \sigma B_0^2 u, \end{aligned} \quad (2)$$

Fig. 1 Geometry of the flow



$$\begin{aligned} \rho C_p v_0 \frac{dT}{dy} &= k \frac{d^2 T}{dy^2} + \mu \left(1 + \Gamma^2 \left(\frac{du}{dy} \right)^2 \right)^{\left(\frac{n-1}{2}\right)} \left(\frac{du}{dy} \right)^2 \\ &+ \mu(n-1)\Gamma^2 \left(1 + \Gamma^2 \left(\frac{du}{dy} \right)^2 \right)^{\left(\frac{n-3}{2}\right)} \left(\frac{du}{dy} \right)^4 \quad (3) \\ &+ \sigma B_0^2 u^2, \end{aligned}$$

and the corresponding conditions have the forms:

$$\begin{aligned} u = 0, \quad k \frac{dT}{dy} &= h_1(-T_2 + T), \quad \text{at } y = 0, \\ u = 0, \quad k \frac{dT}{dy} &= -h_2(T - T_1), \quad \text{at } y = h. \end{aligned} \quad (4)$$

Here, u is the component of velocity in x -direction, μ viscosity coefficient, k thermal conductivity, ρ fluid density, p pressure, σ electrical conductivity, n positive constant, Γ is the material fluid parameter, B_0 constant magnetic field strength, T_2 hot fluid temperature, T_1 ambient temperature, T temperature and h_1, h_2 coefficients of convective heat transport.

Dimensionless form of Eqs. (2)–(4) is given as follows:

$$\left(1 + (f')^2 n W_c^2 \right) \left(1 + (f')^2 W_c^2 \right)^{\left(\frac{n-3}{2}\right)} f'' - \text{Re} f' - M^2 f + P = 0, \quad (5)$$

$$\begin{aligned} \theta'' - \text{Re Pr } \theta' + \text{Ec Pr} \\ \left[\left(1 + (f')^2 n W_c^2 \right) \left(1 + (f')^2 W_c^2 \right)^{\left(\frac{n-3}{2}\right)} (f')^2 + M^2 f^2 \right] &= 0, \end{aligned} \quad (6)$$

with

$$\begin{aligned} f = 0, \quad \theta' - \text{Bi}_1(\theta - 1) &= 0 \quad \text{at } \eta = 0, \\ f = 0, \quad \theta' + \text{Bi}_2(\theta) &= 0 \quad \text{at } \eta = 1. \end{aligned} \quad (7)$$

The above-said equations are obtained upon using following dimensionless variables:

$$u = \frac{\mu}{\rho h} f(\eta), \quad \eta = \frac{y}{h}, \quad \theta = \frac{T - T_1}{T_2 - T_1}. \quad (8)$$

In Eqs. (5–7), $P = \frac{\rho h^3}{\mu^2} \left(-\frac{dp}{dx} \right)$ is the pressure gradient parameter, $\text{We} = \frac{\mu \Gamma}{\rho h^2}$ the Weissenberg number, $\text{Re} = \frac{\rho v_0 h}{\mu}$ Reynolds number, $M = \sqrt{\frac{\sigma B_0^2 h^2}{\mu}}$ magnetic parameter, $\text{Pr} = \frac{\mu C_p}{k}$ Prandtl number, $\text{Ec} = \frac{\mu^2}{h^2 \rho^2 C_p (T_2 - T_1)}$ Eckert number and $\text{Bi}_i = \frac{-h h_i}{k}$ for $i = 1, 2$ Biot number.

The dimensionless skin friction coefficient and Nusselt number are given by:

$$\begin{aligned} \text{Cf} &= \frac{\rho h^2 \tau_w}{\mu^2} = \left\{ 1 + \text{We} [f'(1)]^2 \right\}^{\frac{n-1}{2}} f'(1) \quad \text{and} \\ \text{Nu} &= \frac{h q_m}{k_f (T_2 - T_1)} = -\theta'(1), \end{aligned} \quad (9)$$

$$\begin{aligned} \text{where } \tau_w &= \left\{ \mu \left[1 + \Gamma^2 \left(\frac{du}{dy} \right)^2 \right]^{\frac{n-1}{2}} \frac{du}{dy} \right\}_{y=1} \quad \text{and} \\ q_m &= -k \left(\frac{dT}{dy} \right)_{y=1}. \end{aligned}$$

Entropy analysis

The temperature and velocity fields are utilized for the computation of the rate of entropy production within the microchannel. In the transport of non-Newtonian Carreau fluid due to microchannel, the entropy production must include irreversibility created by viscous heating, Joule heating and heat transport.

$$\begin{aligned} E_g &= \frac{k}{T_1^2} \left(\frac{dT}{dy} \right)^2 + \frac{1}{T_1} \left[\mu \left(1 + \Gamma^2 \left(\frac{du}{dy} \right)^2 \right)^{\left(\frac{n-1}{2}\right)} \left(\frac{du}{dy} \right)^2 \right. \\ &\quad \left. + \mu(n-1)\Gamma^2 \left(1 + \Gamma^2 \left(\frac{du}{dy} \right)^2 \right)^{\left(\frac{n-3}{2}\right)} \left(\frac{du}{dy} \right)^4 + \sigma B_0^2 u^2 \right]. \end{aligned} \quad (10)$$

The local entropy production rate is described as:

$$\begin{aligned} N_s &= \frac{E_g}{E_0} = (\theta')^2 + \text{Ec Pr} \\ &\quad \left[\left(1 + n W_c^2 (f')^2 \right) \left(1 + W_c^2 (f')^2 \right)^{\left(\frac{n-3}{2}\right)} (f')^2 + M^2 f^2 \right], \end{aligned} \quad (11)$$

where $E_0 = \frac{k(T_2 - T_1)^2}{h^2 T_1^2}$ classifies the characteristics entropy generation rate and $L = \frac{T_1}{T_2 - T_1}$ is the characteristic temperature ratio.

Equation (11) can be expressed as:

$$N_s = N_v + N_h. \quad (12)$$

The first term denotes the entropy generation by the heat transport irreversibility, and the second term denotes the entropy generation by viscous dissipation. To examine the irreversibility distribution, the constraint Be (Bejan number) is used. This number is the ratio of entropy production by heat transport to overall entropy generation and can be described as

$$\text{Be} = \frac{N_h}{N_h + N_v}. \quad (13)$$

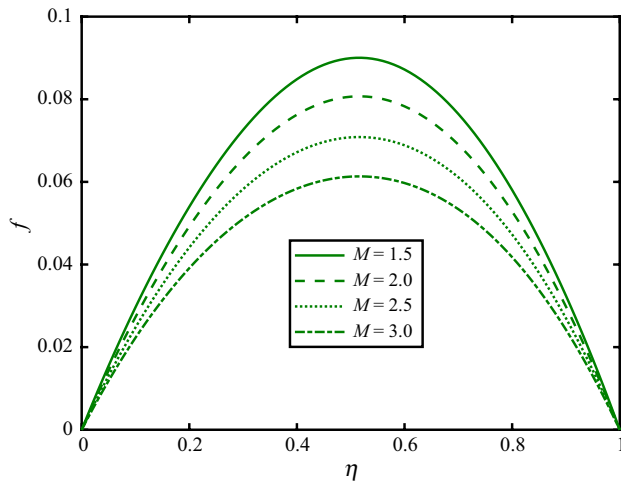


Fig. 2 Effect of M on velocity

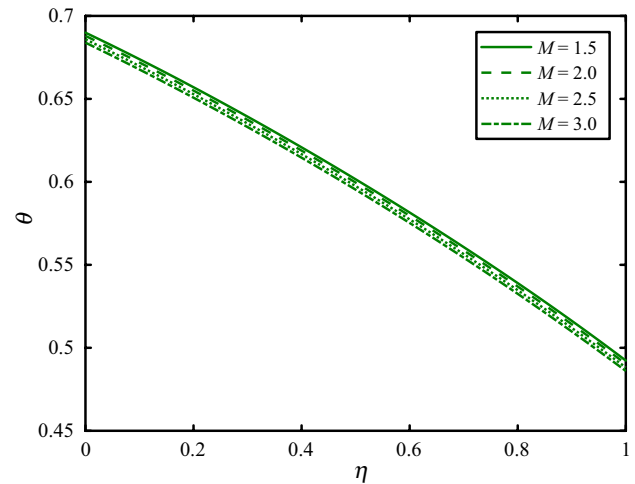


Fig. 3 Effect of M on temperature

Finite element analysis

The nonlinear coupled differential expressions (5) and (5) having conditions (6) are executed through finite element procedure. The whole flow domain is divided into 1000 linear elements having equal size. The complete domain has 1001 nodes because every element is two noded. We developed a system of expressions which has 2002 equations. The developed system is nonlinear, due to which an iterative technique is implemented in the solution. The system of expressions is reduced to 1998 expressions after the implementation of conditions. Subsequent system is treated under accuracy of 10^{-5} by using the Gauss elimination scheme.

Results and discussion

Finite element scheme is introduced to evaluate the solutions of constructed mathematical expressions. These solutions are executed by plotting graphs of distinct constraints values on important quantities from physical point of view. Plots are labeled for distinct constraints to examine the nature of velocity f , temperature θ , rate of local entropy minimization N_s and Bejan number Be . Default values of various parameters are fixed as

$We = 2$, $M = 1.5$, $n = 1.5$, $Re = 0.5$, $Ec = 0.2$, $P = 1$, $Bi = 0.5$.

Figures 2–5 demonstrate the behavior of curves of velocity f , temperature θ , rate of local entropy minimization N_s and Bejan number Be against the distinct values of magnetic field constraint M . Figure 2 clearly executes that the velocity f of liquid reduces by improving the values of magnetic constraint. The curves of velocity f achieve the peak at $\eta = 0.5$. Temperature θ is decayed by enhancing magnetic constraint

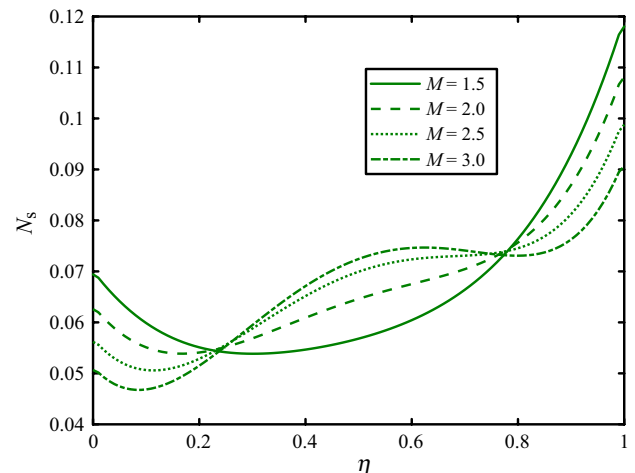


Fig. 4 Effect of M on N_s

M (Fig. 3). A comparative examination of these two figures reports that the change in velocity is more prominent as we found in temperature. This behavior of velocity and temperature is due to existence of Lorentz force factor in magnetic constraint. This factor has dominant nature with the increasing trend of magnetic constraint that produces reduction in the profiles. Figure 4 shows that the local rate of entropy generation N_s has sinusoidal behavior against the incrementing values of magnetic constraint M . The local entropy minimization rate has both increasing and decreasing nature in various parts of microchannel. The impact of magnetic constraint on Bejan number is contrary as we observed for N_s (Figs. 4 and 5). The behavior of Reynolds number Re on velocity f , temperature θ , rate of local entropy minimization N_s and Bejan number Be is visualized in Figs. 6–9.

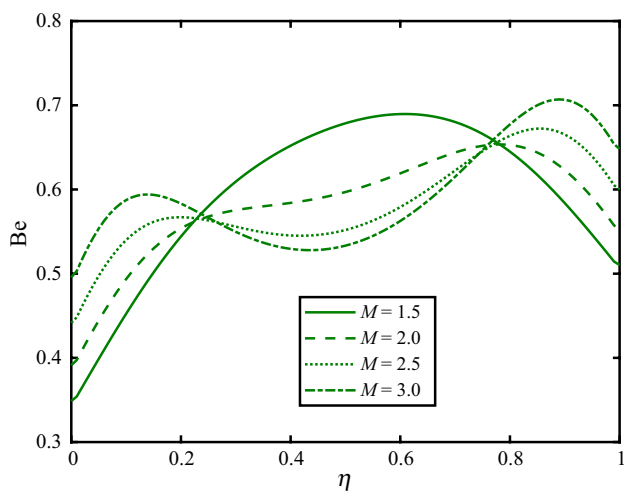


Fig. 5 Effect of M on Be

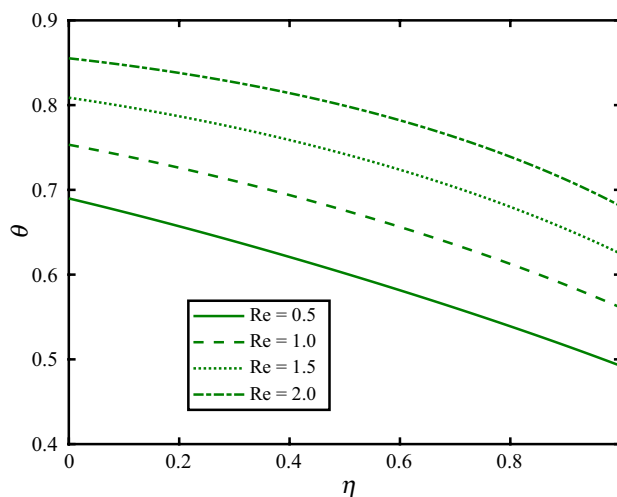


Fig. 7 Effect of Re on temperature

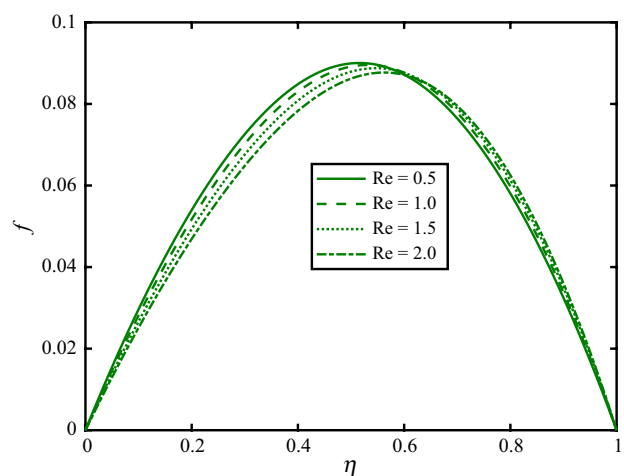


Fig. 6 Effect of Re on velocity

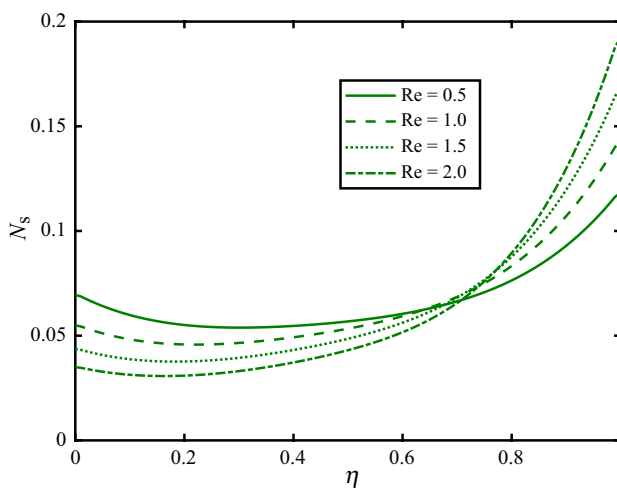


Fig. 8 Effect of Re on N_s

The velocity of liquid becomes the weaker at first half of microchannel, but it starts to improve in the second part at velocity f , temperature θ , rate of local entropy minimization N_s and Bejan number $\eta = 0.61$ against the incrementing values of Re (Fig. 6). Figure 7 explains that the larger temperature curve is visualized against the higher Reynolds number. Temperature at channel wall is also enhanced for incrementing Reynolds number values. Figure 8 reflects that the curves have both increasing and decreasing nature for improving Reynolds number. The decreasing nature is noticed in profiles of N_s up to $\eta = 0.7$, and after that, it starts to boost. The curves of Be demonstrate the similar trend as of N_s for incrementing Reynolds number (Figs. 8 and 9).

The role of Weissenberg number We on velocity f , temperature θ , rate of local entropy minimization N_s and Bejan number Be is characterized in Figs. 10–13. Figures 10 and

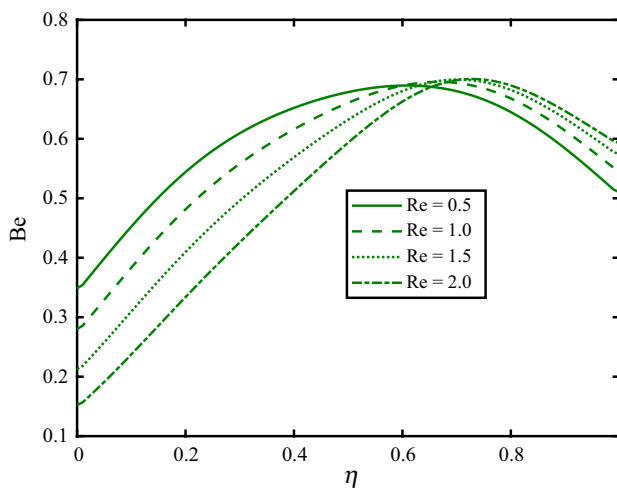


Fig. 9 Effect of Re on Be

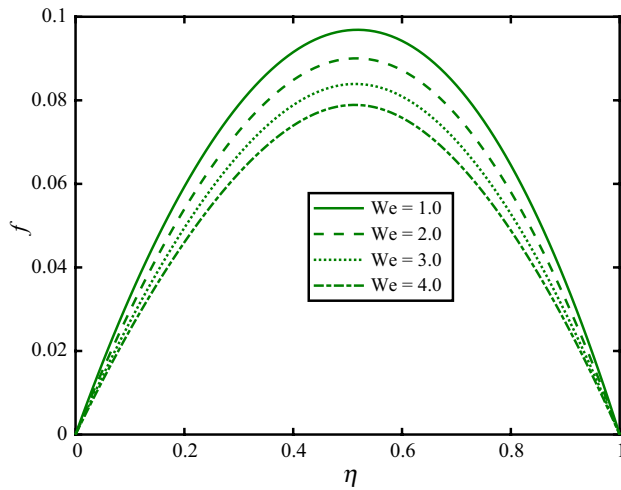


Fig. 10 Effect of We on velocity

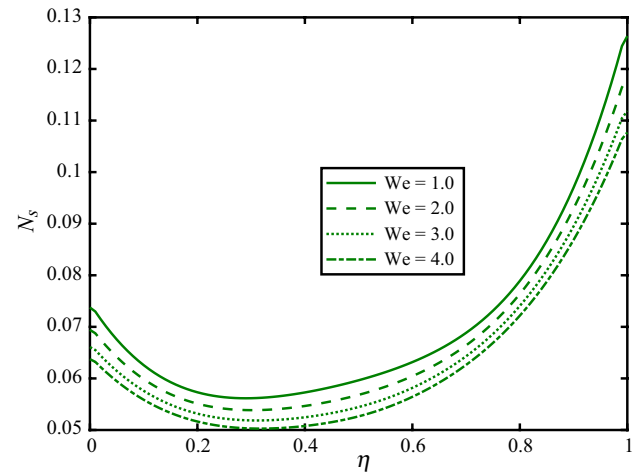


Fig. 12 Effect of We on N_s

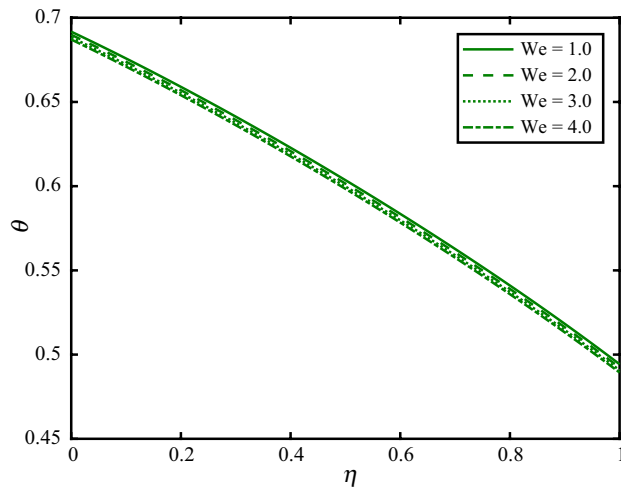


Fig. 11 Effect of We on temperature

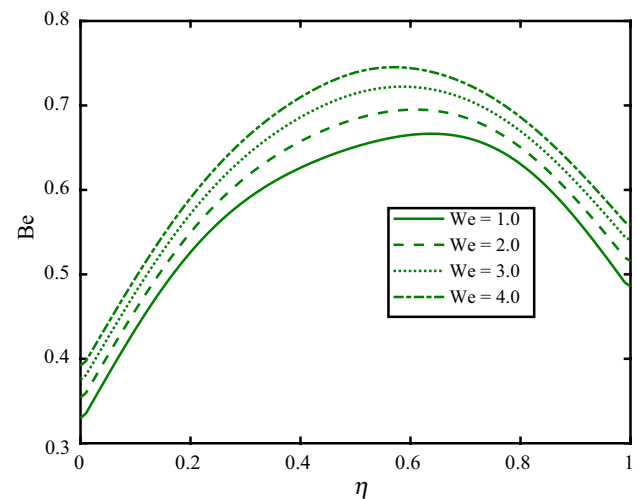


Fig. 13 Effect of We on Be

11 reflect that the curves of velocity f and temperature θ have decreasing behavior for larger Weissenberg number. The curve of velocity is at maximum peak at $\eta = 0.6$. This trend is due to stronger material factor Γ . This factor is directly connected with Weissenberg number, and larger Weissenberg number corresponds to stronger material factor. This stronger material factor is responsible for decrement in the velocity and temperature of liquid. The behavior of Weissenberg number on N_s and Be profiles is quite reverse. The increasing trend of Weissenberg number reduces the

profile of N_s while boosting the curves of Be (Figs. 12 and 13). The behaviors of temperature θ , rate of local entropy minimization N_s and Bejan number Be for distinct Eckert number Ec are addressed in Figs. 14–16. Temperature θ is boosted for larger Eckert number. The internal energy factor is higher for larger Ec due to which heat of liquid is augmented that improves the temperature profiles in Fig. 14. Figures 15 and 16 declare that the larger Eckert number Ec leads to higher N_s and lower Be profiles. From these figures, we recognized that the local entropy generation rate

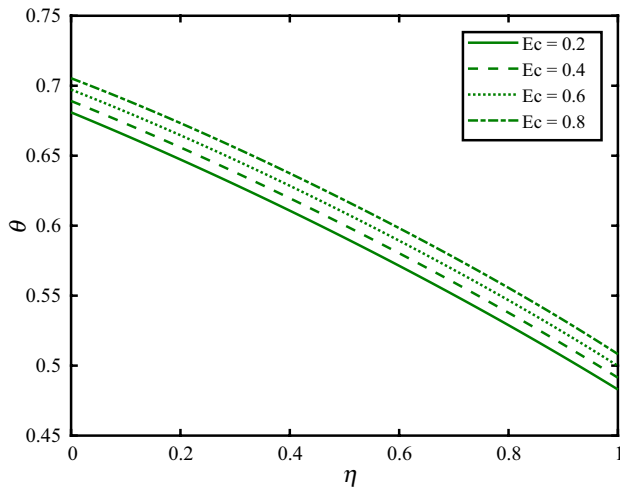


Fig. 14 Effect of Ec on temperature

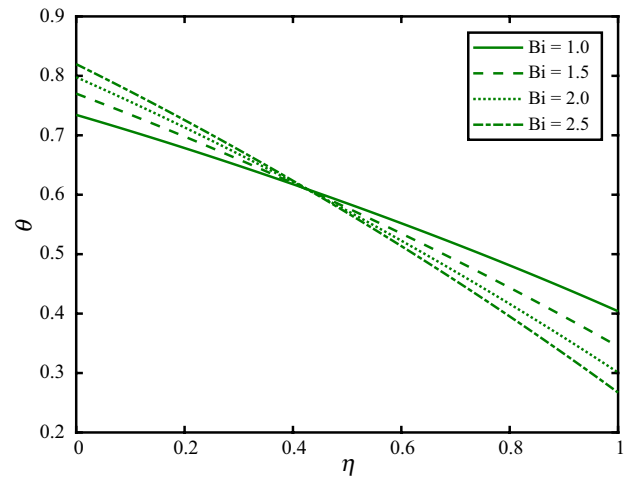


Fig. 17 Effect of Bi on temperature

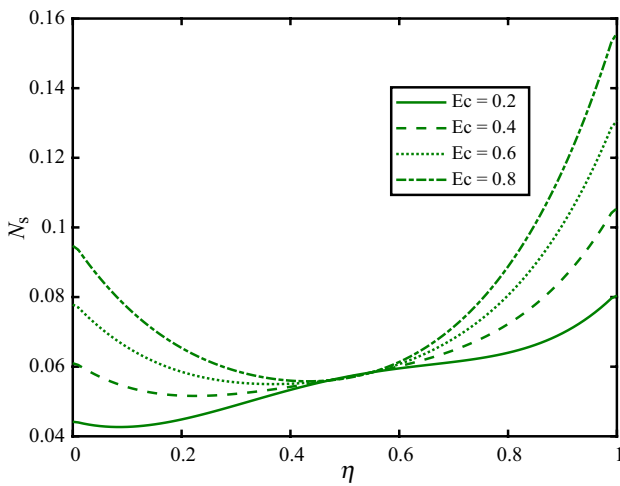


Fig. 15 Effect of Ec on N_s

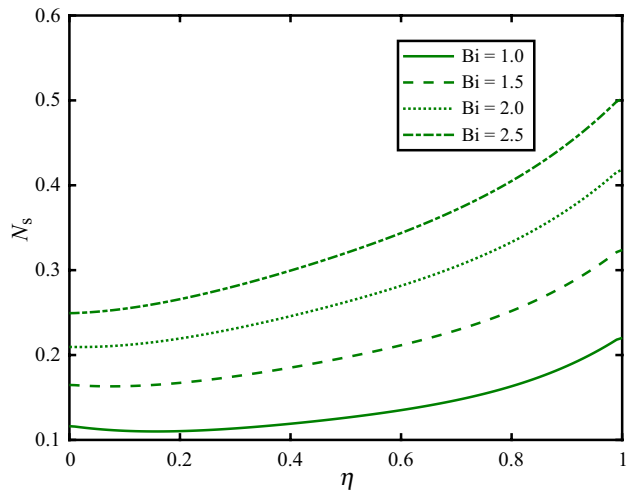


Fig. 18 Effect of Bi on N_s

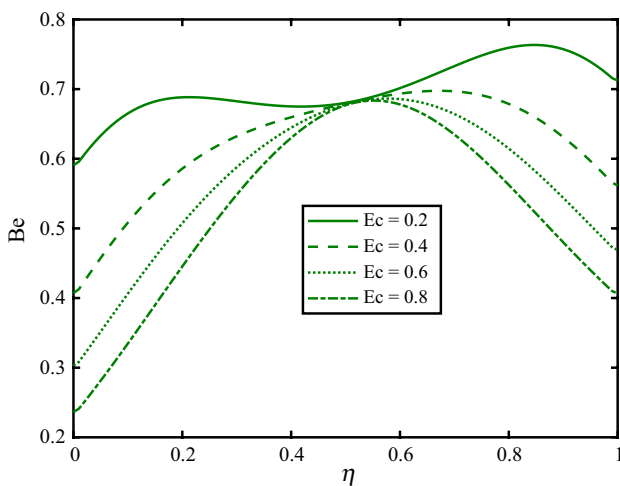


Fig. 16 Effect of Ec on Be

and Bejan number behavior is stable for certain portion of the channel.

Figures 17–19 are displayed to characterize the trend of Biot number Bi on temperature θ , rate of local entropy minimization N_s and Bejan number Be . Figure 17 reveals that the temperature is improved in the first part and decayed in the second part of channel for the increasing Biot number values. The behavior of temperature is changed from higher to lower at $\eta = 0.4$. The local entropy generation N_s and Bejan number Be are higher corresponding to incremented values of Biot number (Figs. 18 and 19). Both the quantities are also boosted at the channel wall for larger Biot number values. The effects of pressure gradient constraint P on velocity f , temperature θ , rate of local entropy minimization N_s and Bejan number

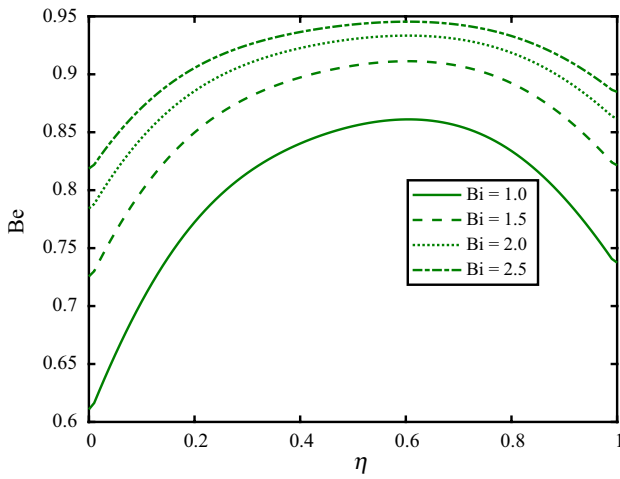


Fig. 19 Effect of Bi on Be

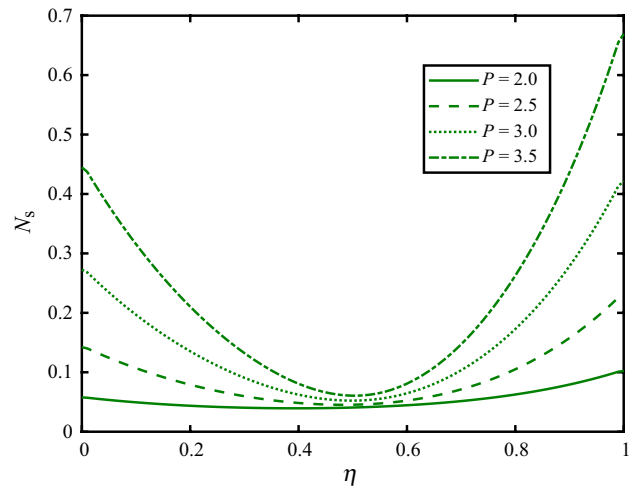


Fig. 22 Effect of P on N_s

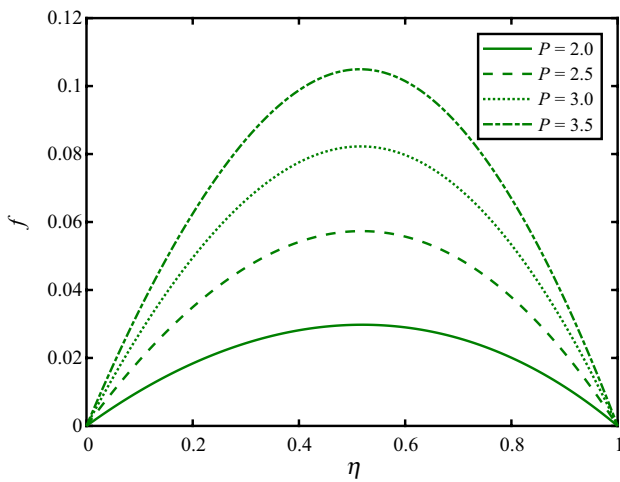


Fig. 20 Effect of P on velocity

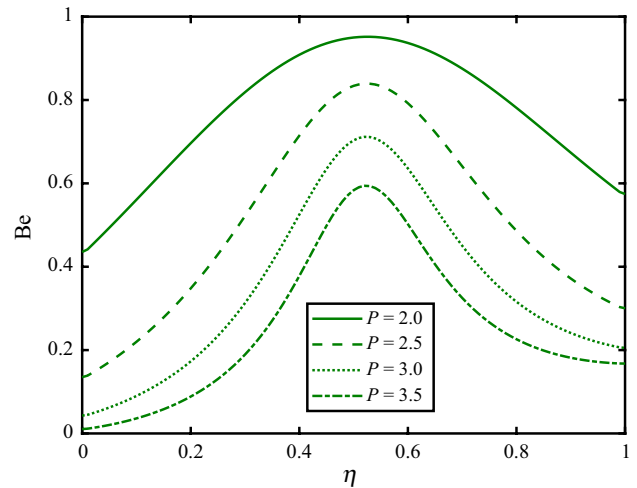


Fig. 23 Effect of P on Be

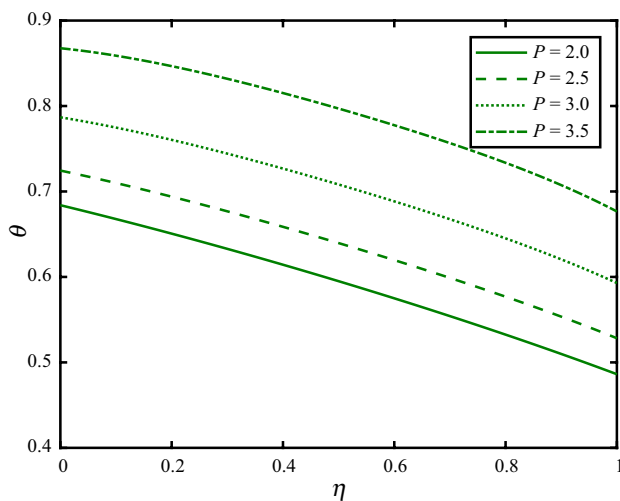


Fig. 21 Effect of P on temperature

Be are reported in Figs. 20, 21, 22, 23. These figures address that the velocity f , temperature θ and rate of local entropy minimization N_s are boosted by enhancing the pressure gradient constraint, but the profiles of Bejan number are decaying for rising pressure gradient constraint. The significance of n on velocity, temperature, rate of local entropy minimization and Bejan number are reported in the Figs. 24, 25, 26, 27 correspondingly. These figures reveal that the velocity, temperature and rate of local entropy minimization are enhanced via stronger values of n whereas the Bejan number declined for increasing values of n . Impact of M on skin friction coefficient and Nusselt number is unpacked in Figs. 28, 29 respectively. Here both skin friction coefficient and Nusselt number are decreasing functions of M . Fig. 30 shows that the Nusselt number increases with Ec .

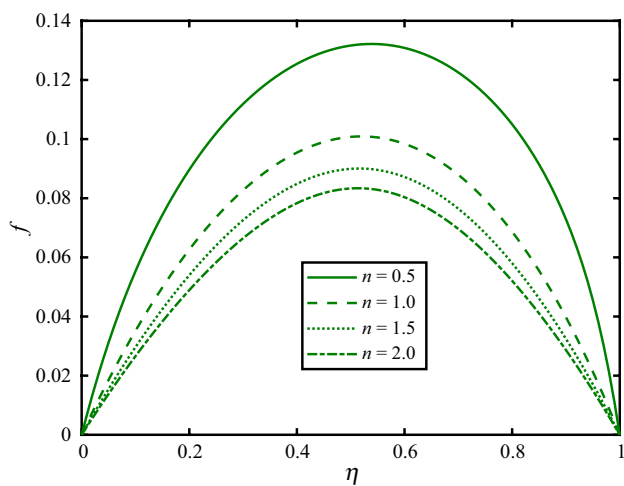


Fig. 24 Effect of n on velocity

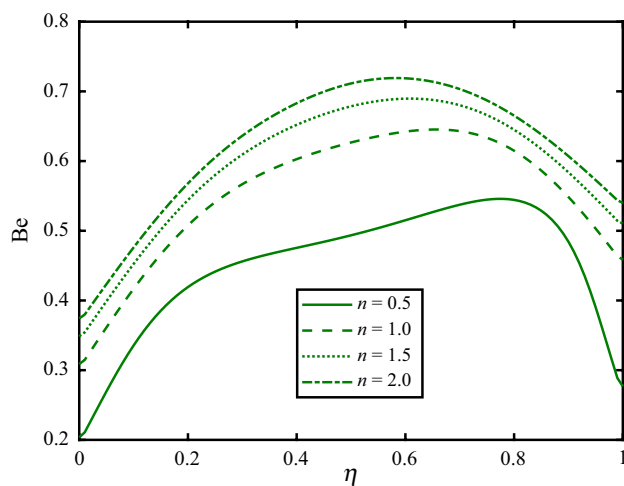


Fig. 27 Effect of n on Be

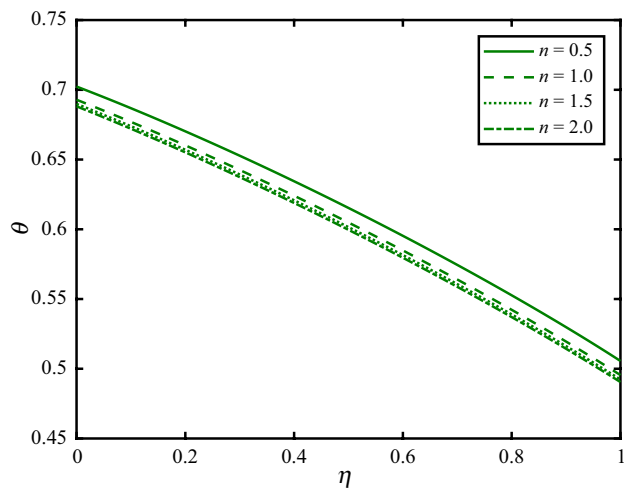


Fig. 25 Effect of n on temperature

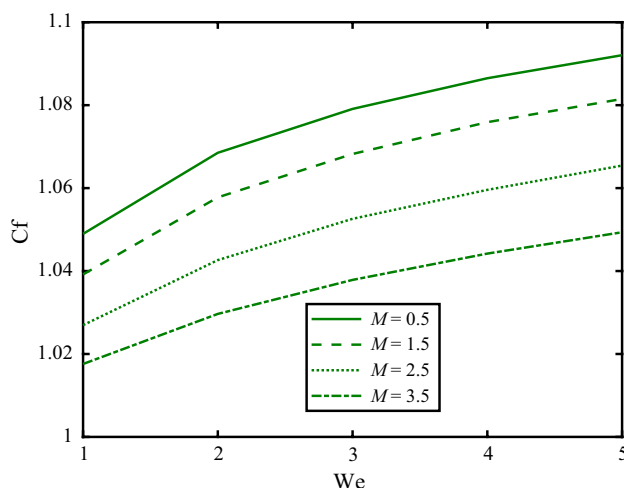


Fig. 28 Effect of We and M on skin friction coefficient

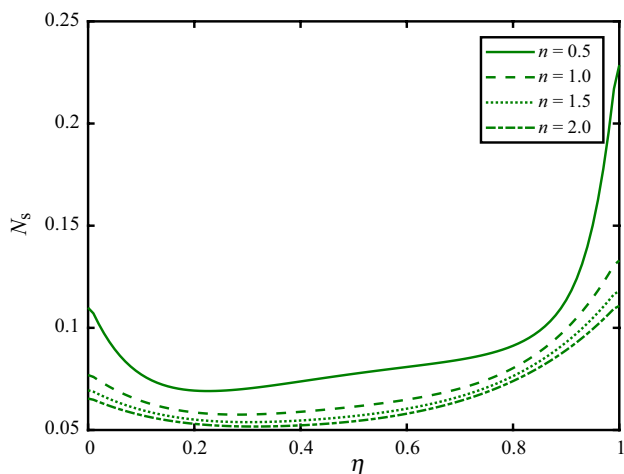


Fig. 26 Effect of n on N_s

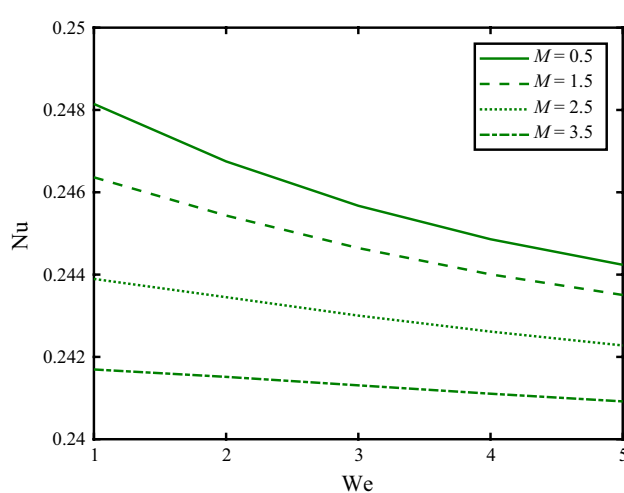


Fig. 29 Effect of We and M on Nusselt number

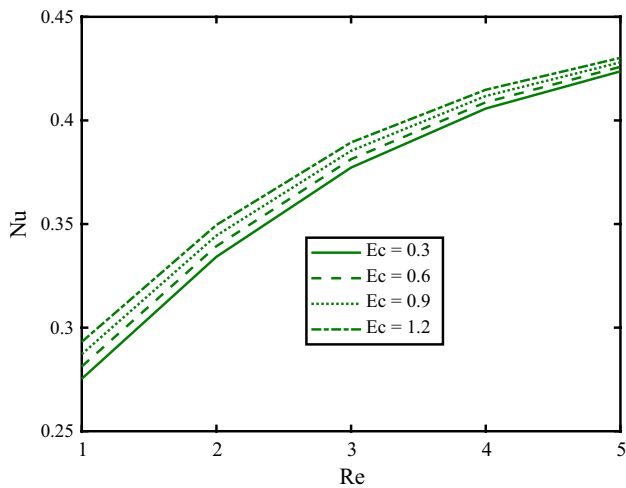


Fig. 30 Effect of Re and Ec on Nusselt number

Concluding remarks

The thermal and entropy generation nature in magneto-Carreau non-Newtonian material induced by convectively heated microchannel has been addressed. Finite element-based numerical scheme is adopted for the solutions of physical model. The results of various quantities are addressed by plotting graphs. It is noted that the Bejan number Be and rate of local entropy generation N_s have sinusoidal nature for increasing values of magnetic field constraint M . The velocity f of liquid is reduced first, but it starts to boost up after $\eta = 0.6$ for increasing trend of Reynolds number Re . The behaviors of N_s and Be for increasing Re are similar in a qualitative way. Both quantities decreased firstly and then boost up when the values of η increased from 0.7. Temperature θ is retarded for larger values of We . The increasing trend of Weissenberg number leads to lower curves of local entropy generation N_s . The Biot number improves the profile of local entropy generation N_s and Bejan number Be . An increase in pressure gradient constraint enhances the velocity profile dramatically in the microchannel.

Acknowledgements One of the authors (Macha Madhu) acknowledges the UGC for the financial support under the Dr. D.S. Kothari Postdoctoral Fellowship Scheme (No. F.4-2/2006 (BSR)/MA/16-17/0043). Also, another author (Mahanthesh B) expresses his sincere thanks to The Management, CHRIST (Deemed to be University) for their kind support to complete this work.

References

- Akbar NS, Nadeem S, Haq RU, Ye S. MHD stagnation point flow of Carreau fluid toward a permeable shrinking sheet: dual solutions. *Ain Shams Eng J.* 2014;5(4):1233–9.
- Khan M, Azam M, Alshomrani A. Effects of melting and heat generation/absorption on unsteady Falkner–Skan flow of Carreau nanofluid over a wedge. *Int J Heat Mass Transf.* 2017;110:437–46.
- Khan M, Azam M, Alshomrani AS. On unsteady heat and mass transfer in Carreau nanofluid flow over expanding or contracting cylinder with convective surface conditions. *J Mol Liq.* 2017;231:474–84.
- Gireesha BJ, Kumar PS, Mahanthesh B, Shehzad SA, Rauf A. Nonlinear 3D flow of Casson–Carreau fluids with homogeneous–heterogeneous reactions: a comparative study. *Results Phys.* 2017;7:2762–70.
- Hsiao KL. To promote radiation electrical MHD activation energy thermal extrusion manufacturing system efficiency by using Carreau–Nanofluid with parameters control method. *Energy.* 2017;130:486–99.
- Khan M, Azam M. Unsteady heat and mass transfer mechanisms in MHD Carreau nanofluid flow. *J Mol Liq.* 2017;225:554–62.
- Chaffin ST, Rees JM. Carreau fluid in a wall driven corner flow. *J Non-Newtonian Fluid Mech.* 2018;253:16–26.
- Kefayati GR, Tang H. MHD thermosolutal natural convection and entropy generation of Carreau fluid in a heated enclosure with two inner circular cold cylinders, using LBM. *Int J Heat Mass Transf.* 2018;126:508–30.
- Hayat T, Ahmed B, Abbasi FM, Alsaedi A. Numerical investigation for peristaltic flow of Carreau–Yasuda magneto-nanofluid with modified Darcy and radiation. *J Therm Anal Calorim.* 2019;137(4):1359–67.
- Waqas H, Khan SU, Bhatti MM, et al. Significance of bioconvection in chemical reactive flow of magnetized Carreau–Yasuda nanofluid with thermal radiation and second-order slip. *J Therm Anal Calorim.* 2020;140:1293–1306. <https://doi.org/10.1007/s10973-020-09462-9>.
- Chamkha AJ, Rashad AM, Armaghani T, Mansour MA. Effects of partial slip on entropy generation and MHD combined convection in a lid-driven porous enclosure saturated with a Cu–water nanofluid. *J Therm Anal Calorim.* 2018;132(2):1291–306.
- Mehryan SA, Izadi M, Chamkha AJ, Sheremet MA. Natural convection and entropy generation of a ferrofluid in a square enclosure under the effect of a horizontal periodic magnetic field. *J Mol Liq.* 2018;263:510–25.
- Shamsabadi H, Rashidi S, Esfahani JA. Entropy generation analysis for nanofluid flow inside a duct equipped with porous baffles. *J Therm Anal Calorim.* 2019;135(2):1009–19.
- Seyyedi SM, Dogonchi AS, Ganji DD, Hashemi-Tilehnoee M. Entropy generation in a nanofluid-filled semi-annulus cavity by considering the shape of nanoparticles. *J Therm Anal Calorim.* 2019;138(2):1607–21.
- Abbasi FM, Shanakhat I, Shehzad SA. Entropy generation analysis for peristalsis of nanofluid with temperature dependent viscosity and Hall effects. *J Magn Magn Mater.* 2019;474:434–41.
- Shafee A, Haq RU, Sheikholeslami M, Herki JA, Nguyen TK. An entropy generation analysis for MHD water based Fe_3O_4 ferrofluid through a porous semi annulus cavity via CVFEM. *Int Commun Heat Mass Transf.* 2019;108:104295.
- Abbasi FM, Shanakhat I, Shehzad SA. Analysis of entropy generation in peristaltic nanofluid flow with Ohmic heating and Hall current. *Phys Script.* 2019;94(2):025001.
- Sheikholeslami M. New computational approach for exergy and entropy analysis of nanofluid under the impact of Lorentz force through a porous media. *Comput Methods Appl Mech Eng.* 2019;344:319–33.
- Bahrami A, Safavinejad A, Amiri H. Analysis of spectral radiative entropy generation in a non-gray planar participating medium at radiative equilibrium with two different boundary conditions. *Int J Therm Sci.* 2019;146:106073.

20. Hayat T, Ahmad MW, Khan MI, Alsaedi A. Entropy optimization in CNTs based nanomaterial flow induced by rotating disks: a study on the accuracy of statistical declaration and probable error. *Compu Methods Progr Biom.* 2020;184:105105.
21. Monaledi RL, Makinde OD. Entropy analysis of a radiating variable viscosity EG/Ag nanofluid flow in microchannels with buoyancy force and convective cooling. *Defect Diffus Forum.* 2018;387:273–85.
22. Das S, Jana RN, Makinde OD. MHD flow of Cu–Al₂O₃/water hybrid nanofluid in porous channel: analysis of entropy generation. *Defect Diffus Forum.* 2017;377:42–61.
23. Gireesha BJ, Srinivasa CT, Shashikumar NS, Macha M, Singh JK, Mahanthesh B. Entropy generation and heat transport analysis of Casson fluid flow with viscous and Joule heating in an inclined porous microchannel. *Proc Inst Mech Eng Part E J Process Mech Eng.* 2019;233(5):1173–84.
24. Khan ZH, Makinde OD, Ahmad R, Khan WA. Numerical study of unsteady MHD flow and entropy generation in a rotating permeable channel with slip and Hall effects. *Commun Theor Phys.* 2018;70(5):641.
25. Shashikumar NS, Prasannakumara BC, Archana M, Gireesha BJ. Thermodynamics analysis of a Casson nanofluid flow through a porous microchannel in the presence of hydrodynamic slip: a model of solar radiation. *J Nanofluids.* 2019;8(1):63–72.
26. Ma X, Sheikholeslami M, Jafaryar M, Shafee A, Nguyen-Thoi T, Li Z. Solidification inside a clean energy storage unit utilizing phase change material with copper oxide nanoparticles. *J Clean Prod.* 2020;245:118888.
27. Venkateswarlu M, Prameela M, Makinde OD. Influence of heat generation and viscous dissipation on hydromagnetic fully developed natural convection flow in a vertical micro-channel. *J Nanofluids.* 2019;8(7):1506–16.
28. Venkateswarlu M, Makinde OD, Lakshmi DV. Influence of thermal radiation and heat generation on steady hydromagnetic flow in a vertical micro-porous-channel in presence of suction/injection. *J Nanofluids.* 2019;8(5):1010–9.
29. Monaledi RL, Makinde OD. inherent irreversibility in Cu–H₂O nanofluid Couette flow with variable viscosity and nonlinear radiative heat transfer. *Int J Fluid Mech Res.* 2019;46(6):525–43.
30. Madhu M, Shashikumar NS, Mahanthesh B, Gireesha BJ, Kishan N. Heat transfer and entropy generation analysis of non-Newtonian flu flow through vertical microchannel with convective boundary condition. *Appl Math Mech.* 2019;40(9):1285–300.
31. Shashikumar NS, Gireesha BJ, Mahanthesh B, Prasannakumara BC, Chamkha AJ. Entropy generation analysis of magneto-nanoliquids embedded with aluminium and titanium alloy nanoparticles in microchannel with partial slips and convective conditions. *Int J Numer Methods Heat Fluid Flow.* 2018;29(10):3638–58.
32. Madhu M, Shashikumar NS, Gireesha BJ, Kishan N. Second law analysis of Powell–Eyring fluid flow through an inclined microchannel with thermal radiation. *Phys Scr.* 2019;94(12):125205.

Publisher's Note Springer Nature remains neutral with regard to jurisdictional claims in published maps and institutional affiliations.